Plasma Chemistry and Plasma Processing (2024) 44:1735–1752
https://doi.org/10.1007/s11090-024-10464-w

ORIGINAL PAPER

Production of Alkaline Plasma Activated Tap Water Using Different Plasma Forming Gas at Sub-Atmospheric Pressure

Vikas Rathore[1] · Karaket Watanasit[2] · Suttirak Kaewpawong[2] · Dhammanoon Srinoumm[2] · Arlee Tamman[3] · Dheerawan Boonyawan[4] · Mudtorlep Nisoa[2,5]

Received: 3 November 2023 / Accepted: 3 March 2024 / Published online: 10 May 2024

Abstract
The present study demonstrates the successful production of alkaline plasma-activated tap water (PATW), effectively addressing the challenge of acidity in traditional PATW for a range of applications. Through precise control of plasma-forming gases (oxygen, air, argon) and process parameters, particularly by producing PATW under sub-atmospheric pressure conditions, it becomes possible to shift the pH of acidic PATW towards the alkaline range. This transformation enhances its suitability for applications like agriculture, aquaculture, sterilization, wound healing, disinfection, and food preservation, etc.

The investigation encompassed the characterization of plasma and the identification of various plasma species/radicals. The impact of different plasma-forming gases on the pH of PATW and the concentration of reactive species in PATW was thoroughly analyzed. Plasma generated using oxygen and argon resulted in the production of reducing or alkaline PATW, while the use of air and air-argon mixtures led to an acidic or oxidizing nature.

The study also discussed the stability of nitrate ions, nitrite ions, and hydrogen peroxide in PATW, shedding light on their behavior over varying plasma treatment times and plasma-forming gas. Finally, the investigation explored the effects of gas flow rates, gas pressures, water volume, and plasma discharge powers on the concentration of H_2O_2 in PATW, providing valuable insights into optimizing the production process.

Keywords Plasma-activated tap Water · Alkaline Water · Reactive oxygen-nitrogen Species · Emission Spectra · Different plasma-forming Gases

Introduction

Plasma-Activated Water (PAW) is an emerging plasma technology that demonstrates substantial potential across a diverse range of applications, from sterilization to agriculture. Previous researchers have explored various applications of PAW, including sterilization, food preservation, selective elimination of cancer cells, medicinal uses (e.g., wound healing), inactivation of pathogens (bacteria, fungi, viruses, pests), enhancement of seed germi-

Extended author information available on the last page of the article

nation and plant growth, and as a nitrogen source in agriculture and aquaculture [1–19]. For instance, Raud et al. [1] demonstrated decreased cell viability in breast and prostate cancer cell lines following PAW treatment. Wang et al. [2] reported superior wound healing ability of PAW in a mouse full-thickness skin wound model.

Ten Bosch et al. [7] previously explored the insecticidal efficacy of PAW, reporting a high mortality rate of approximately 90% among insects after 24 h of treatment. Guo et al. [6] investigated the virus inactivation mechanism by PAW. They highlighted that oxidizing species, such as single oxygen, damage the structure of various viruses, including double-stranded DNA, single-stranded DNA, and RNA bacteriophages. Consequently, virus inactivation occurs post-PAW treatment.

Our previously published reports discuss diverse applications of PAW in antimicrobial, antifungal, food preservation, agriculture, and aquaculture [3, 4, 8–10]. In experiments, a few seconds of PAW exposure led to over a 6+CFU ml^{-1} log reduction in pathogenic bacteria such as *Staphylococcus aureus* and *Pseudomonas aeruginosa* [8]. Additionally, brief PAW exposure completely inhibited pathogenic fungi, including *Candida albicans* and the food spoilage agent *Citrus limon* fungi [4]. Washing Citrus limon with PAW extended its shelf life by over two months while preserving sensory and nutritional properties [3].

Our previous research also indicated that PAW treatment enhances seed germination and plant growth in peas (*Pisum sativum* L.), with seeds treated showing a 37% increase in germination and a 95% increase in plant growth compared to the control group [9]. Additionally, PAW can serve as a nitrogen source for freshwater algae growth, showing up to 626% increase compared to conventional Bold's Basal Medium [10].

The effectiveness of PAW in various applications can be attributed to the presence of diverse reactive oxygen-nitrogen species. Components like H_2O_2, dissolved O_3, $ONOO^-$, etc., play a crucial role in microbial inactivation, food preservation, wound healing, and other applications. Furthermore, the existence of reactive nitrogen species, such as NO_3^- ions and NO_2^-, establishes PAW as an environmentally friendly nitrogen source for agriculture and aquaculture [20–24].

Reports on the physicochemical properties of PAW by numerous researchers indicate its acidic and oxidizing nature, which is integral to its activities in disinfection, sterilization, food preservation, etc. The acidic nature of PAW results from the formation of nitrous and nitric acid during plasma-water interactions, as evidenced by the increased concentration of H^+ ions, NO_3^- ions, and NO_2^- ions [25–34].

However, the acidic pH of PAW poses challenges for medicinal and agricultural applications, impacting crop health, soil health, and overall environmental balance. Low pH solutions are not recommended for medicinal use due to their potential to oxidize skin cells upon contact, leading to damage and skin irritation, as well as eye irritation [35–37].

In food preservation, a low pH solution may oxidize the outer surface of food, leading to a loss in nutritional value, texture, taste, and overall food quality. Likewise, in agriculture, the low pH of PAW is a concern as it can significantly impact crop health and soil health, considering the desired pH range for agricultural and aquaculture applications is neutral to slightly basic (6.5 to 8) [38–40]. Sivachandiran et al. [41] also demonstrated that high exposure of plasma to water makes the water acidic, negatively affecting seed germination and plant growth.

Moreover, during surface sterilization or disinfection, the low pH of PAW can cause problems such as rusting and corrosion, etc. [42–44]. Nevertheless, the acidic solution waste

leads to soil and water acidification, which can harm aquatic life, plants, and the ecosystem. Hence, the use of a low pH solution always comes with environmental regulatory compliance for proper use and exploitation [38–40].

This study addresses these concerns and introduces a novel approach for producing alkaline plasma-activated tap water (PATW). Previously, Pang et al. [45] highlighted the significance of alkaline plasma-activated water in cancer treatment. However, their method involved using an alkaline sodium hydroxide solution for the production of alkaline PAW. In contrast, the present study endeavors to produce alkaline PAW utilizing commonplace household tap water. A sub-atmospheric pressure vacuum system has been designed and developed to enable large-volume production of plasma-activated alkaline tap water. The generation of PATW utilizes a radio frequency (RF) power source. Characterization of PATW involves studying changes in pH and the concentrations of reactive oxygen and nitrogen species, including nitrate ions, nitrite ions, and hydrogen peroxide. Additionally, the study highlights the effects of different plasma-forming gases and their combinations on the properties of PATW.

Materials and Methods

The production process of plasma-activated tap water (PATW) is illustrated in Fig. 1. To achieve alkaline water production, preventing interference from nitrogen molecules in the surrounding air is crucial. The discharge of nitrogen plasma species results in the formation of nitrous and nitric acid in the water, significantly lowering its pH and undermining the study's objective. Consequently, all experiments were conducted under sub-atmospheric pressure (also known as negative pressure or vacuum), facilitated by a vacuum pump. Figure 1 depicts the vacuum chamber, boasting a volume of 5 L. The vacuum in the system ($\sim 10^{-2}$ torr) was created using a Joto 2BV2060 vacuum pump [46]. The base gas (air, Ar, O_2) pressure varies from 36 to 49 torr.

The plasma electrode, a critical component for plasma generation, was crafted from stainless steel and was positioned within the vacuum chamber. It was energized by a high-voltage radio frequency (RF) power supply, reaching a maximum power of 500 W. The voltage and frequency range for this power supply were 1 to 10 kV and 50 to 500 kHz, respectively. Plasma-forming gases, including air, argon (Ar), and oxygen (O_2), were introduced into the vacuum chamber, with the flow rate of the feed gas being controlled using a flow controller. The voltage-current waveform was monitored using an oscilloscope, and plasma species/radicals were identified using a spectrometer in the range of 290 to 875 nm, respectively.

In the preparation of PATW, 100 to 500 ml of tap water was placed in a cup within the vacuum chamber for activation. The gas flow rate varied from 0 to 8 L min^{-1} (air, O_2, Ar, air+Ar). The electrode was energized with a frequency of 20 kHz and 0 to 500 W RF power to activate the water. Cooling for the chamber was achieved by utilizing metallic pipes containing cooling water wrapped around the vacuum chamber, connected to a water chiller, as illustrated in Fig. 1.

Monitoring the pH of PATW was carried out using a pH meter (Mettler Toledo Seven Compact pH/Ion meter). The determination of reactive oxygen-nitrogen species (RONS) such as NO_2^- ions, NO_3^- ions and H_2O_2 in PATW was conducted semi-quantitatively

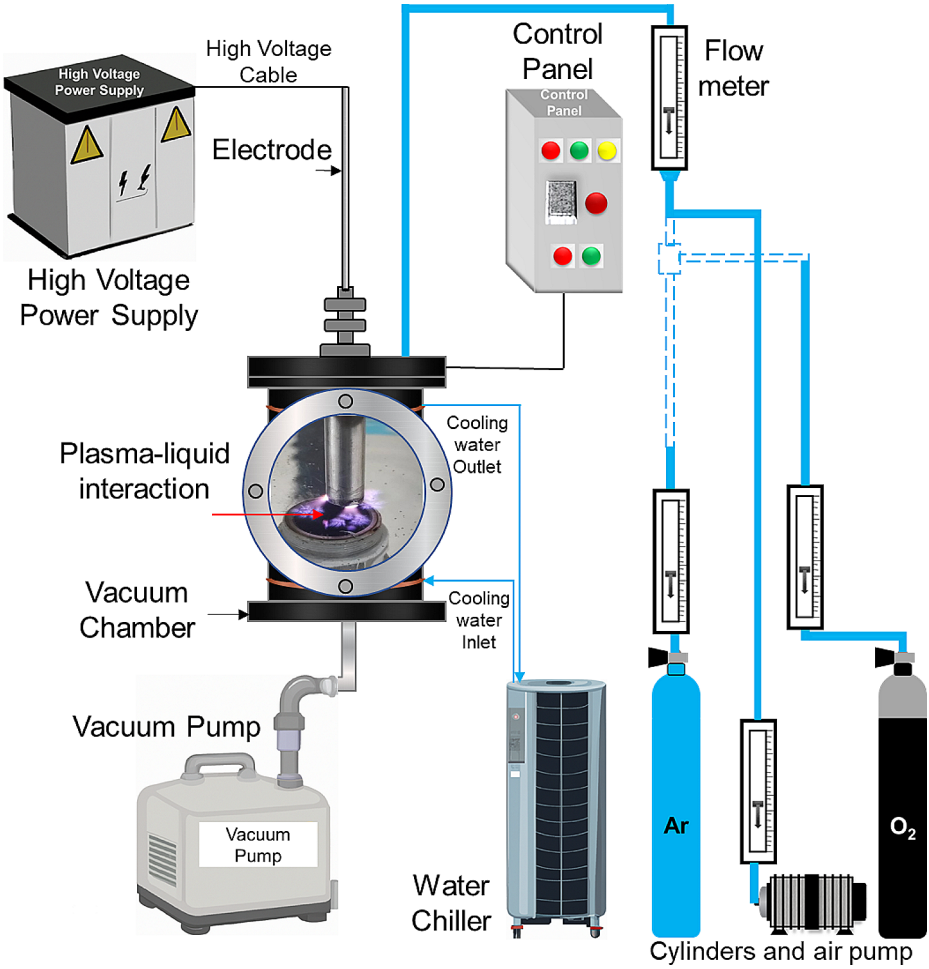

Fig. 1 Schematic of the high-volume plasma-activated tap water production process

employing MACHEREY-NAGEL QUANTOFIX semi-quantitative test strips. The test strips used were MACHEREY-NAGEL QUANTOFIX NO_3^-/NO_2^- ions for NO_3^- and NO_2^- ions determination, and MACHEREY-NAGEL QUANTOFIX Peroxide for H_2O_2 determination. The temperature of the water was measured using a mercury thermometer.

Results and Discussion

Plasma Characterization

Voltage-Current Waveform

Figure 2 illustrates the voltage-current waveform of air plasma generated during plasma-water interaction under sub-atmospheric pressure within the vacuum chamber. The recorded peak-to-peak voltage was 13.4 kV, displaying a sinusoidal waveform (see Fig. 2). The non-uniform dielectric barrier filamentary discharges were noticeable during the plasma-water interaction, as depicted in Fig. 1 within the vacuum chamber. This observation was supported by the presence of multiple peaks representing current filaments in Fig. 2. These current filaments indicate the formation of various reactive species and radicals during air discharge in each rising and falling current half-cycle [47]. The resulting radicals and species dissolved in water during the plasma-water interaction give rise to plasma-activated water [6, 15, 18, 19, 22, 26, 48–50].

Identification of Plasma Species/Radicals

Figure 3 illustrates the emission spectra of air plasma, argon plasma, oxygen plasma, and air + argon plasma under sub-atmospheric conditions, providing insights into their impact on various physicochemical properties and the concentration of reactive species in PATW.

In Fig. 3(a), the emission spectra of air plasma primarily exhibit strong vibrational band peaks from nitrogen gas (N_2) of the second (2nd) positive system (N_2 ($C\ ^3\Pi_u \rightarrow B\ ^3\Pi_g$)) (Eqs. (1–2)). This is accompanied by the N_2^+ first negative system (N_2^+ ($B\ ^2\Sigma_u^+ \rightarrow X\ ^2\Sigma_g^+$)) (Eqs. (3–4)), hydroxyl radical rotational band, and hydrogen lines. The observed OH ($A\ ^2\Sigma \rightarrow X\ ^2\Pi$) and H_α lines indicate the dissociation of H_2O molecules (air moisture) to form OH and H (Eqs. (10–11) [51–55]. The excited N_2 and N_2^+, along with OH and H, interact with the various reactive oxygen-nitrogen species in PATW (Eqs. (5–11, 14–25)) [8, 29, 49, 56–73]. The observed emission spectra in Fig. 3(a) represent the radiative decay transition of N_2, N_2^+, OH band peaks, and the H_α line (Eqs. (2, 4, 10)). The strong electric field (high voltage) applied accelerates the electrons, exciting, ionizing, and dissociating the N_2, O_2, H_2O, etc., atoms/molecules present in the air (Eqs. (1–11)). The emission intensity of

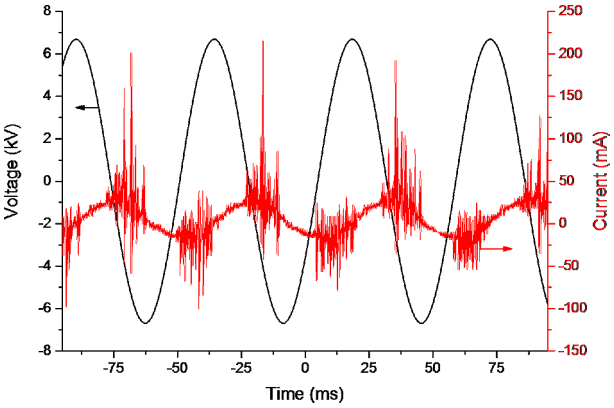

Fig. 2 Voltage-current waveform of air plasma generated under sub-atmospheric pressure

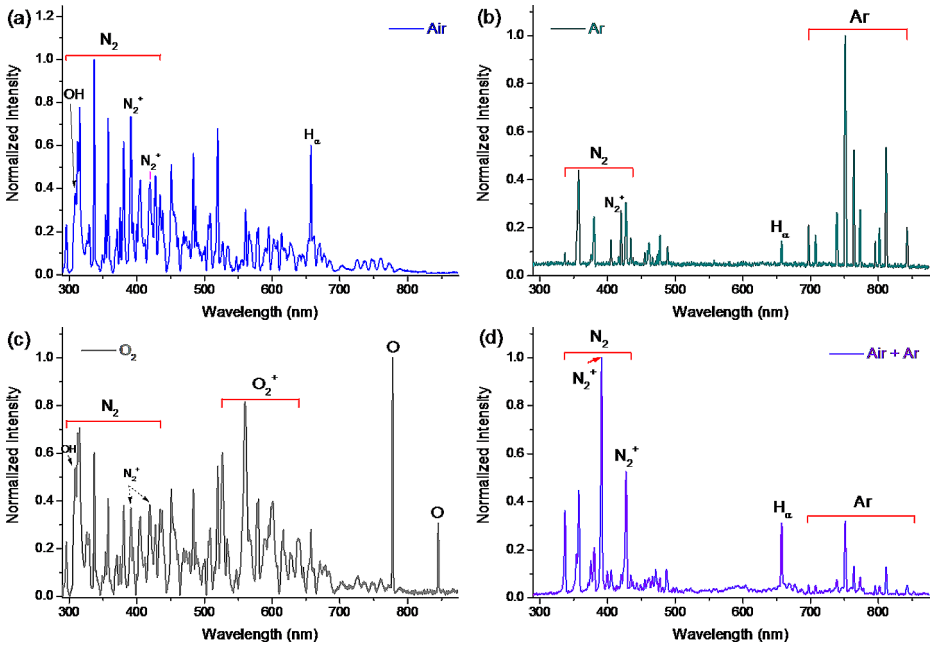

Fig. 3 Emission spectra of (**a**) Air, (**b**) Argon (Ar), (**c**) Oxygen (O_2) gas, and (**d**) Air+Ar gas mixture produced under sub-atmospheric pressure

observed emission band peaks N_2, N_2^+, OH, and H_α line dominates over other species/radicals formed during air discharge (Eqs. (2, 4, 10)). As a result, their domination is observed only in Fig. 3 (a).

Figure 3(b) displays the emission spectra of argon (Ar) plasma, characterized by strong emission lines of atomic Ar (4p → 4s) in the range of 680 to 850 nm (Eqs. (12–13)) [66, 74], along with relatively weak vibrational band peaks from N_2 ($C\ ^3\Pi_u \rightarrow B\ ^3\Pi_g$) and N_2^+ ($B\ ^2\Sigma_u^+ \rightarrow X\ ^2\Sigma_g^+$) systems, and the H_α line (Eqs. (2, 4, 10)). The observed nitrogen vibrational band peaks and the H_α line were attributed to nitrogen and moisture impurities present in the vacuum chamber under sub-atmospheric pressure.

In Fig. 3(c), the emission spectra of oxygen (O_2) plasma predominantly feature a strong atomic line of atomic oxygen (O (3p → 3s)) [75], accompanied by vibrational band peaks from the N_2 ($C\ ^3\Pi_u \rightarrow B\ ^3\Pi_g$) and N_2^+ ($B\ ^2\Sigma_u^+ \rightarrow X\ ^2\Sigma_g^+$) systems, and O_2^+ first negative system ($b\ ^4\Sigma_g \rightarrow a\ ^4\Pi_u$) (Eqs. (2, 4, 6–8)) [76]. The emission lines and molecular band peaks of oxygen dominate in oxygen plasma along with air impurities in the form of nitrogen and hydroxyl molecular band peaks (Fig. 3(c)).

When air was introduced into argon plasma, Fig. 2(d) illustrates a significant reduction in the emission intensity of atomic argon lines (Ar (4p → 4s)), indicating the dominance of N_2 and N_2^+ emission vibrational band peaks (N_2 ($C\ ^3\Pi_u \rightarrow B\ ^3\Pi_g$) and N_2^+ ($B\ ^2\Sigma_u^+ \rightarrow X\ ^2\Sigma_g^+$)) over argon lines. Furthermore, the moisture content present in the inserted air enhances the intensity of the H_α line in comparison to Ar plasma (Fig. 2 (d)).

Physicochemical Properties and Concentration of Reactive Species in PATW

The plasma species and radicals discussed above, generated using various plasma-forming gases, undergo changes in the physicochemical properties of water when they contact water inside the vacuum chamber [18, 50, 59, 61, 65, 66]. These alterations are depicted in Fig. 4. PATW production utilizing O_2 and Ar as plasma-forming gases indicates the generation of alkaline or reducing PATW. Conversely, when air and an air+Ar mixture were used for PATW production, an acidic or oxidizing nature was observed.

This variation in pH is due to the formation of different reactive species in different concentrations. The acidic PATW is dominated by oxidizing species like a high concentration of H^+, NO_2^-, NO_3^-, H_2O_2, etc., whereas reducing PATW has a high concentration of reducing species like HO^- or a lower concentration of oxidizing species like NO_2^-, NO_3^-, H_2O_2, etc. [49, 64, 66, 71–73].

The proposed reactions occur in the reactive plasma phase [51–55, 66, 74]:

$$N_2(X) + e^- \rightarrow N_2(C) + e^- \tag{1}$$

$$N_2(C) \rightarrow N_2(B) + hv \tag{2}$$

$$N_2(X) + e^- \rightarrow N_2^+(B) + 2e^- \tag{3}$$

$$N_2^+(B) \rightarrow N_2^+(X) + hv \tag{4}$$

$$N_2 + e^- \rightarrow 2N + e^- \tag{5}$$

$$O_2 + e^- \rightarrow O_2^+ + 2e^- \tag{6}$$

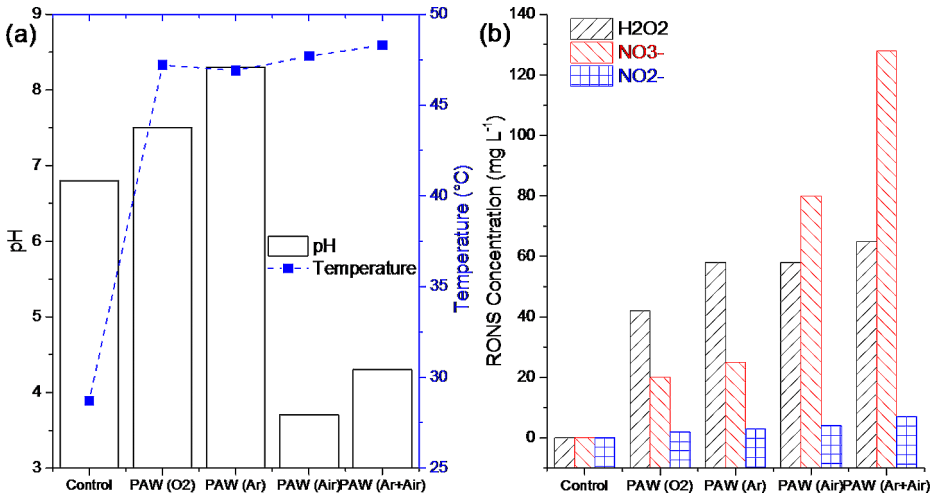

Fig. 4 Impact of various plasma-forming gases on physicochemical properties (**a**) pH and concentration of reactive species (**b**) nitrate ($NO3^-$) ions, nitrite ($NO2^-$) ions, and hydrogen peroxide (H_2O_2) in PATW

$$O_2^+(b) \rightarrow O_2^+(a) + hv \tag{7}$$

$$O_2 + e^- \rightarrow 2O + e^- \tag{8}$$

$$xO + yN \underrightarrow{M} N_yO_x(NO, NO_2, NO_3, N_2O_5, etc.) \tag{9}$$

$$H_2O \underrightarrow{M} H + OH \tag{10}$$

$$OH(A) \rightarrow OH(X) + hv \tag{11}$$

Only occurs in Ar plasma:

$$Ar + e^- \rightarrow Ar^* + e^- \tag{12}$$

$$Ar(p) \rightarrow Ar(s) + hv \tag{13}$$

The proposed reactions occur in the reactive liquid phase [8, 29, 49, 56–73]:

$$H \cdot \underrightarrow{M} \boldsymbol{H}^+ + e^- \tag{14}$$

$$OH + OH \rightarrow \boldsymbol{H_2O_2} \tag{15}$$

$$NO_2 + e^- \rightarrow \boldsymbol{NO_2^-} \tag{16}$$

$$NO_3 + e^- \rightarrow \boldsymbol{NO_3^-} \tag{17}$$

$$H^+ + NO_2^- \leftrightharpoons HNO_2 \tag{18}$$

$$H^+ + NO_3^- \leftrightharpoons HNO_3 \tag{19}$$

$$\boldsymbol{NO_2^-} + \boldsymbol{H_2O_2} + H^+ \rightarrow ONOOH + H_2O \rightarrow \boldsymbol{NO_3^-} + H^+ + H_2O \tag{20}$$

$$OH + e^- \rightarrow \boldsymbol{OH^-} \tag{21}$$

$$2OH^- + NO \rightarrow \boldsymbol{NO_2^-} + H_2O \tag{22}$$

$$2OH^- + NO \rightarrow \boldsymbol{NO_3^-} + H_2 \tag{23}$$

$$HNO_3 + OH^- \rightarrow \boldsymbol{NO_3^-} + H_2O \tag{24}$$

$$HNO_2 + OH^- \rightarrow \boldsymbol{NO_2^-} + H_2O \tag{25}$$

Where '*M*' represents high-energy third bodies, energetic electrons, radiation, etc. providing an energetic environment for reactions to occurs in both the plasma phase and liquid phase.

The pH of PATW produced using air and Ar as plasma-forming gases exhibited the minimum (acidic) and maximum (basic) values compared to other plasma-forming gases. The corresponding values were 3.7 and 8.3, respectively. Additionally, plasma-water interaction facilitates heat transfer from plasma to water, raising the temperature. To maintain the temperature of Plasma-Activated Tap Water (PATW) below 50 °C, continuous cooling of the vacuum chamber was employed, as illustrated in Fig. 4 (a). The decrease in the pH of water after treatment is in line with previous reported work by Tian et al. [61], Ma et al. [65], and Lu et al. [64], etc.

Figure 4 (b) presents the concentration of various reactive species formed in PATW using different plasma-forming gases. The proposed reactions involved in the formation of these RONS in PATW are shown by Eqs. (14–25) [8, 29, 49, 56–73]. PATW prepared using Ar+Air and Air as plasma-forming gases exhibited a significantly higher concentration of NO_3^- ions compared to other plasma-forming gases. This was attributed to the higher concentration of N_2 carried by the inserted air compared to the presence of air impurities at sub-atmospheric pressure while preparing PATW using O_2 and Ar as plasma-forming gases. The elevated concentration of high-energy N_2 species/radicals reacts with oxygen molecules in the high-energy plasma reactive environment, forming NO_x, which dissolves in water to produce NO_3^- and NO_2^- ions in PATW (Eqs. (16–17)) [8, 14, 23, 32, 57, 64]. Moreover, these NO_3^- and NO_2^- ions combine with H^+ to form nitric (HNO_3) and nitrous acid (HNO_2) in PATW (Eqs. (18–19)) [8, 14, 23, 32, 57, 64]. The H^+ ions were generated through the dissociation of H_2O molecules into H radicals, also evident in the emission spectra as the H_α line (Fig. 3).

Hence, the presence of these acids significantly decreases the pH of PATW when prepared using Air and Air+Ar mixture as a plasma-forming gas, Along with the observed NO_3^- ions in PAW (O_2) and PAW (Ar) were due to air impurities present at sub-atmospheric pressure. However, the formed nitrous and nitric acid were neutralized by the higher concentration of hydroxide ions, as shown in Eqs. (24, 25) [61, 71–73]. Moreover, the presence of hydroxide ions supports the formation of NO_2^- and NO_3^- ions, as shown in Eqs. (22, 23) [61, 71–73].

Moreover, the concentration of NO_2^- ions in PATW prepared using Air and Air+Ar was slightly higher compared to O_2 and Ar. This can be attributed to the highly reactive environment of PATW (Air) and PATW (Air+Ar), attributed to the highly reactive environment promoting the reaction between NO_2^- ions with H_2O_2, resulting in the formation of stable NO_3^- ions as shown in Eq. (20) (32, 56). Consequently, even with an excess of NO_2^- ions compared to PATW (Air) and PATW (Air+Ar), their concentration decreased due to their reactivity with H_2O_2.

The reaction between NO_2^- ions and H_2O_2 also led to a reduction in the concentration of H_2O_2 in PATW (Air) and PATW (Air+Ar) (Eq. (20)) [32, 56]. The presence of moisture in the air increased the concentration of H_2O_2 in PATW (Air)+PATW (Air+Ar), in addition to the moisture from the evaporation of water kept in the vessel inside the vacuum chamber (Eqs. (10, 15)). However, H_2O_2 formed in PATW (O_2) or PATW (Ar) was solely due to the dissociation of residual air moisture and the evaporation of water molecules. Given the low reactivity (neutral or basic pH) and low oxidizing potential of PATW (O_2) or PATW (Ar), the possibility of a reaction between NO_2^- and H_2O_2 was significantly low (Eq. (20)), resulting in little to no degradation of H_2O_2 in PATW (O_2) or PATW (Ar).

Figure 5 illustrates the change in physicochemical properties (pH) and the concentration of reactive species (NO_3^-, NO_2^-, H_2O_2) over varying plasma treatment time with water.

The results demonstrate a notable increase in the pH of water when Ar or O_2 was used for water activation (Fig. 5 (a)), aligning with the discussed findings above. Conversely, a decrease in the pH of water was observed when air was employed as the plasma-forming gas. This decrease in pH with prolonged plasma treatment time was consistent with the previously published literature of Sajib et al. [23], Xiang et al. [63], Shen et al. [59], etc. The heightened pH in PATW (Ar) or PATW (O_2) signifies a substantial increase in the hydroxyl ion concentration with prolonged plasma treatment time (Eq. (21)). The maximum percentage increase in pH for PATW (Ar) and PATW (O_2) compared to the pH of control (tap water) was reported as 41.5% and 44.5%, respectively.

Furthermore, Fig. 5 (b) illustrates the variation in nitrate (NO_3^-) ion concentration in PATW prepared with different plasma-forming gases, correlating with increasing plasma treatment time. The PATW prepared with various gases exhibit a consistent pattern: an initial rise in NO_3^- ion concentration followed by a decrease with prolonged plasma treatment time. This pattern highlights the lower stability of NO_3^- ions in PATW under vacuum conditions. The high-energy electrons from the plasma dissociate the dissolved NO_2^- and NO_3^- ions in PATW to corresponding N_2 and O_2, resulting in a decrease in the concentration of NO_2^- and NO_3^- ions with increasing plasma treatment time. A similar trend was observed in NO_2^- ion concentration, where an initial rise was followed by a continuous decrease in concentration. The highest concentrations of NO_3^- and NO_2^- ions were observed at 10 min of treatment time, recorded as 99.8 mg L^{-1} and 6.95 mg L^{-1} (PATW (Ar)), 40.1 mg L^{-1} and 4.9 mg L^{-1} (PATW (O_2)), and 162.6 mg L^{-1} and 11.0 mg L^{-1} (PATW (Air)). After 10 min

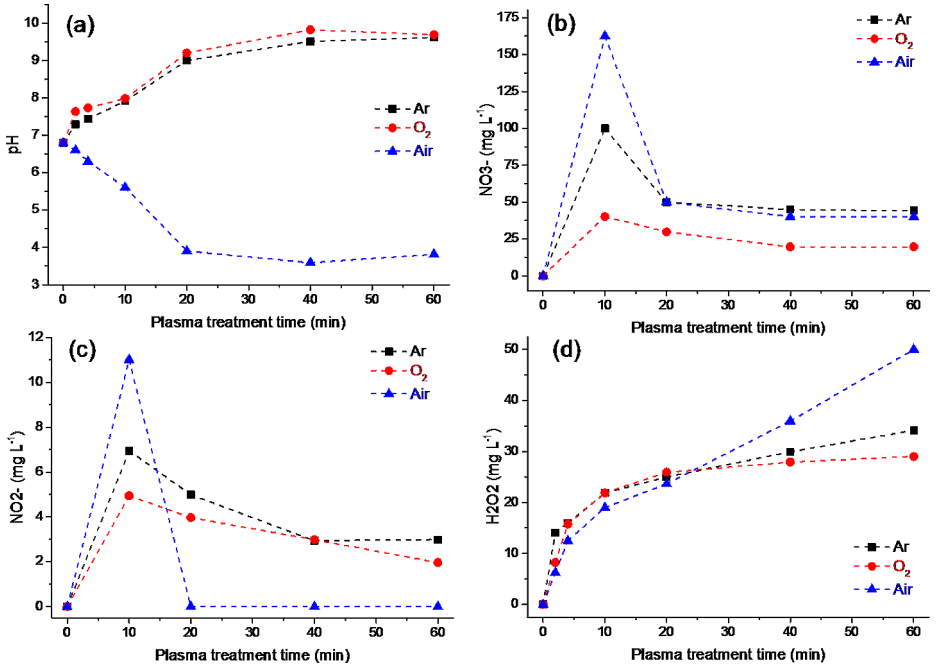

Fig. 5 Impact of plasma treatment duration on physicochemical properties: (**a**) pH, and reactive species concentration: (**b**) nitrate (NO_3^-) ions, (**c**) nitrite (NO_2^-) ions, and (**d**) hydrogen peroxide (H_2O_2) in PATW.

of plasma treatment time, a substantial decrease in the concentration of NO_2^- and NO_3^- ions was observed with increasing plasma treatment time. This was due to the dissociation of NO_2^- and NO_3^- ions by high-energy electrons from the plasma, breaking down the dissolved nitrogen oxide ions into corresponding nitrogen and oxygen gas, which was then removed by the vacuum pump. As a result, the declining nature of NO_2^- and NO_3^- ions was observed in PATW with increasing plasma treatment time (Fig. 5 (b, c)).

The variation in H_2O_2 concentration in PATW prepared using different plasma-forming gases is shown in Fig. 5(d). In this figure, a monotonous increase in H_2O_2 concentration was observed for all plasma-forming gases. This trend was also observed in previously reported works by Tian et al. [61], Lu et al. [64], Arda et al. [14], etc. Additionally, a decrease in H_2O_2 concentration was not observed in PATW (air) with increasing plasma treatment time. This was due to the reducing concentration of NO_2^- and NO_3^- ions in PAW, limiting the reaction between H_2O_2 and NO_2^-. As a result, the decrease in the concentration of H_2O_2 in PATW (air) was not observed, and PAW (air) showed the highest concentration of H_2O_2 compared to other plasma-forming gases.

The graph presented in Fig. 6 illustrates the fluctuation in H_2O_2 concentration within PATW (O_2) and PATW (Ar) as the flow rate varies. An evident trend shows that an increase in plasma-water treatment leads to a consistent rise in H_2O_2 concentration across all specified flow rates for both PATW (O_2) and PATW (Ar) [32, 49, 50]. However, when focusing on PATW (O_2), a noticeable rise and fall in H_2O_2 concentration was observed at different flow rates, as depicted in Fig. 6 (a). The optimal concentration of H_2O_2 (79 mg L^{-1}) in PATW (O_2) was achieved at a flow rate of 4 L min^{-1}. The reduction in H_2O_2 concentration at higher flow rates can be attributed to the reduced discharge of O_2 molecules. This is due to the high molecular density of O_2, causing rapid energy dissipation and reduced ionization, resulting in lower H_2O_2 formation in PATW (O_2) under the given input power.

In contrast, this fluctuating behavior in H_2O_2 concentration was not observed in PATW (Ar). A higher flow rate of Ar, indicative of a higher Ar atom density, results in an elevated

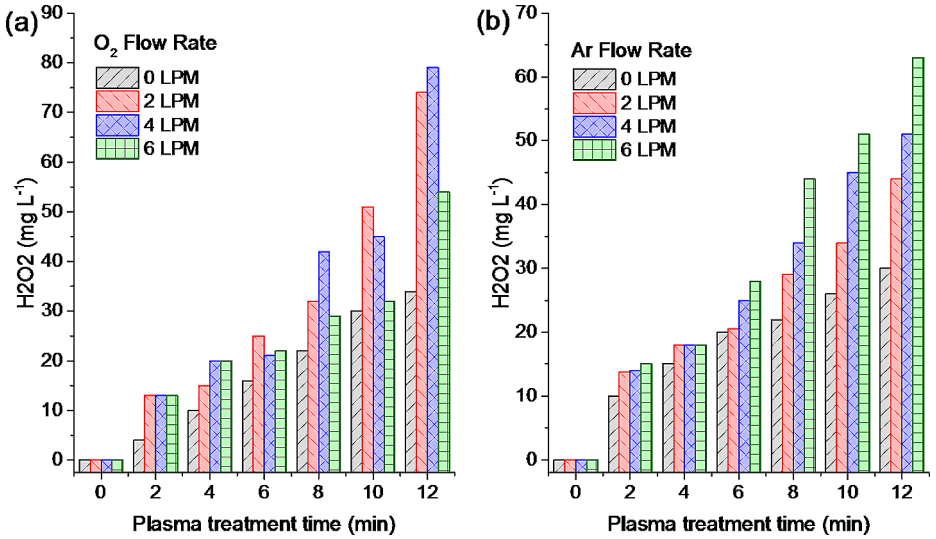

Fig. 6 Variation in H_2O_2 concentration in (**a**) PATW with oxygen (O_2) gas and (**b**) PATW with argon (Ar) gas at different flow rates

concentration of H_2O_2 in PATW (Ar). The supplied energy was sufficient to ionize Ar and other atoms/molecules even at high flow rates, leading to a significant increase in H_2O_2 concentration (63 mg L^{-1}) observed at a flow rate of 6 L min^{-1}.

In Fig. 7 (a), we observe the variation in H_2O_2 concentration within PATW (Ar) under different gas pressures, maintaining a constant plasma power of 105 W. Notably, lower Ar gas pressure (36 torr) demonstrates a significantly higher concentration of H_2O_2 compared to the 76 torr Ar gas pressure. This variance can be attributed to the dissipation of plasma energy by the high density of Ar atoms at elevated gas pressure, consequently reducing the formation of OH radicals. As a result, a lower concentration of H_2O_2 was observed in PATW (Ar) at 76 torr gas pressure.

Additionally, Fig. 7 (b) showcases the impact of increasing plasma discharge power on the H_2O_2 concentration in PATW (Ar). Maintaining a fixed treatment time of 20 min, elevating the plasma discharge power from 24 to 136 W results in a 100% increase in the H_2O_2 concentration in PATW (Ar). This effect is attributed to the heightened plasma power at a consistent gas pressure, promoting increased gas ionization and, consequently, a greater formation of hydroxyl radicals [32, 49, 50]. This increase in hydroxyl radicals is mirrored by the amplified concentration of H_2O_2 in PATW.

Moreover, an extension in plasma treatment time leads to a rise in the water temperature, causing water loss during plasma treatment, as depicted in Fig. 7(a). Initially, the loss of water was considerably higher for low Ar gas pressure (36 torr) compared to high Ar gas pressure (76 torr). However, towards the end of 120 min, the loss of water stabilizes and becomes comparable for both low and high gas pressures.

Figure 8 illustrates the stability of H_2O_2 during storage and its impact on H_2O_2 concentration in PATW (Ar). In Fig. 8 (a), the concentration of H_2O_2 in PATW (Ar) remains comparable for both 200 ml and 500 ml volumes initially, with slight variations observed during a 10-minute treatment. Notably, a significantly higher concentration of H_2O_2 was

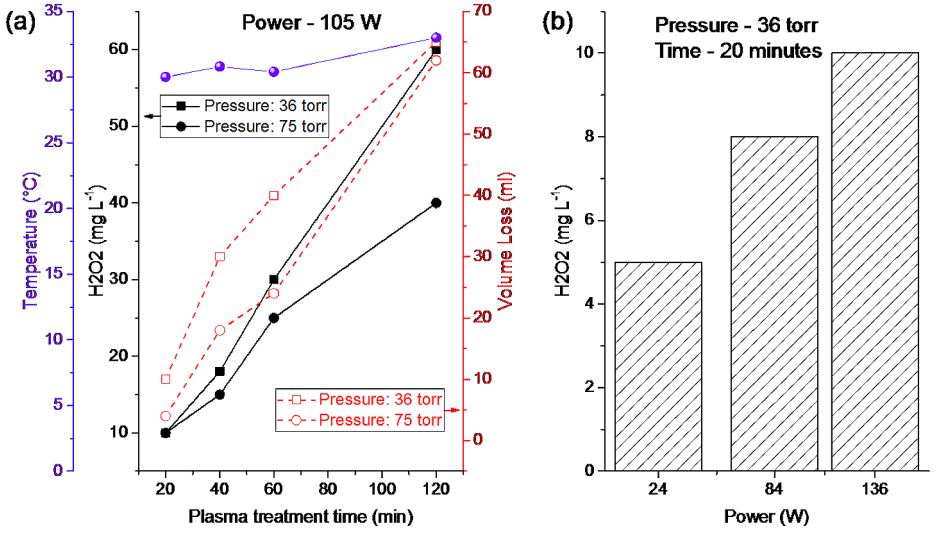

Fig. 7 Variation in H_2O_2 concentration in PATW with respect to gas pressure and power: (**a**) variations in H_2O_2 concentration, temperature, and volume loss in PATW concerning plasma treatment time. (**b**) variation in H_2O_2 concentration with respect to plasma discharge power

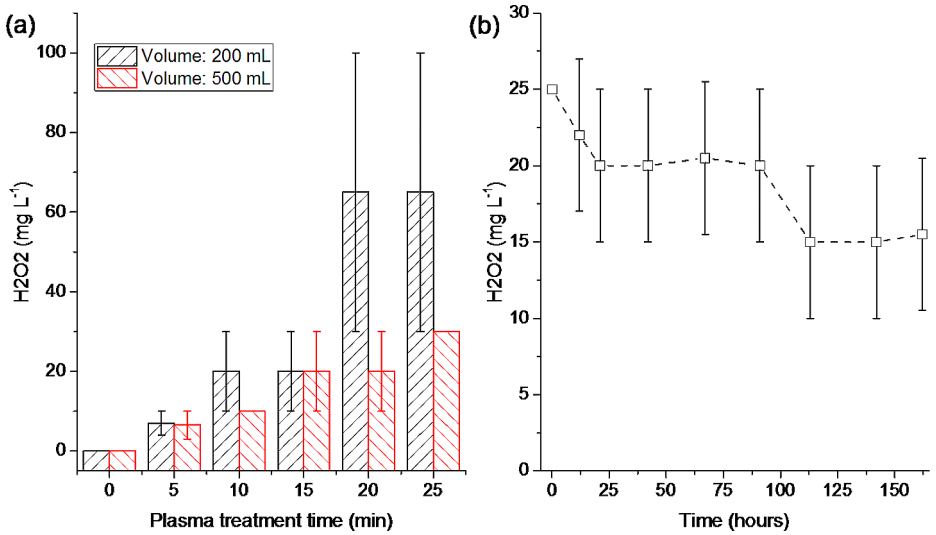

Fig. 8 (**a**) Variations in H_2O_2 concentration in PATW (Ar) with varying volume and (**b**) time-dependent stability of H_2O_2 concentration in PATW (Ar)

observed in the 200 ml PATW compared to the 500 ml PATW at extended plasma-water treatment times. This difference is attributed to the higher H_2O_2 density in the lower volume of PATW compared to the higher volume, while all other process parameters and power remain constant [49].

In Fig. 8 (b), the stability of H_2O_2 in PATW (Ar) over time is presented. After approximately 113 h (around 5 days) from production, a 40% decrease in H_2O_2 concentration was observed. However, between approximately 5 to 7 days (113 to 162 h), there was a 10% increase in H_2O_2 concentration. This fluctuation indicates that after the initial increase and subsequent decrease in H_2O_2 concentration in PATW (Ar), it stabilizes over time [49, 59].

Conclusion

This study has introduced an innovative method for producing alkaline plasma-activated tap water, overcoming the limitations posed by the acidic nature of conventional PATW. Alkaline PATW was prepared using Ar or O_2 as the plasma-forming gas at sub-atmospheric pressure. The concentrations of NO_3^- and NO_2^- were substantially lower compared to air as the plasma-forming gas. However, at high plasma treatment times, a reduction in RNS concentration was observed at sub-atmospheric pressure due to the dissociation of dissolved reactive nitrogen species in PATW. Simultaneously, the concentration of H_2O_2 kept increasing with treatment time using different plasma-forming gases.

Moreover, the gas flow rate, plasma discharge power, volume of water, and gas pressure significantly influence the concentration of dissolved H_2O_2 in PAW. Stability studies showed an initial decrease in H_2O_2 concentration with storage, which then stabilized over time.

In conclusion, these findings contribute to the understanding of plasma-water interactions and offer a promising avenue for tailoring PATW to specific applications, particularly in the realms of agriculture, aquaculture, food preservation, wound healing, disinfection, and sterilization, where a neutral to slightly basic pH is desired. The insights gained pave the way for further advancements and applications in this burgeoning field of plasma-activated water technology.

Acknowledgements We would like to thank Agricultural Research Development Agency (ARDA), International Research Network (IRN), Thailand Institute of Nuclear Technology (TINT) and Walailak university, for their funding supports.

Author Contributions K.W., S.K., D.S., A.T., and M.N. designed and conducted the experiment. M.N. & V.R. analyzed the data and wrote the first draft of the manuscript. D.B. performed the review and editing of the manuscript.

Funding Agricultural Research Development Agency (ARDA), International Research Network (IRN), Thailand Institute of Nuclear Technology (TINT) and Walailak university.

Data Availability All data are will be made available by the corresponding author upon reasonable request.

Declarations

Conflict of Interest Authors have no competing interests.

Ethical Approval Not applicable.

References

1. Raud S, Raud J, Jõgi I, Piller C-T, Plank T, Talviste R et al (2021) The production of plasma activated water in controlled ambient gases and its impact on cancer cell viability. Plasma Chem Plasma Process 41(5):1381–1395
2. Wang S, Xu D, Qi M, Li B, Peng S, Li Q et al (2021) Plasma-activated water promotes wound healing by regulating inflammatory responses. Biophysica 1(3):297–310
3. Rathore V, Nema SK (2023) Enhancement of Shelf Life of Citrus Limon L. (Lemon) using plasma activated Water. Plasma Chem Plasma Process 43:1109–1129
4. Rathore V, Patel D, Shah N, Butani S, Pansuriya H, Nema SK (2021) Inactivation of Candida albicans and lemon (Citrus limon) spoilage fungi using plasma activated water. Plasma Chem Plasma Process 41(5):1397–1414
5. Rashid M, Rashid M, Alam M, Talukder M (2022) Stimulating effects of plasma activated water on growth, biochemical activity, nutritional composition and yield of Potato (Solanum tuberosum L). Plasma Chem Plasma Process. :1–15
6. Guo L, Xu R, Gou L, Liu Z, Zhao Y, Liu D et al (2018) Mechanism of virus inactivation by cold atmospheric-pressure plasma and plasma-activated water. Appl Environ Microbiol 84(17):e00726–e00718
7. Ten Bosch L, Köhler R, Ortmann R, Wieneke S, Viöl W (2017) Insecticidal effects of plasma treated water. Int J Environ Res Public Health 14(12):1460
8. Rathore V, Patel D, Butani S, Nema SK (2021) Investigation of physicochemical properties of plasma activated water and its bactericidal efficacy. Plasma Chem Plasma Process 41:871–902
9. Rathore V, Tiwari BS, Nema SK (2022) Treatment of pea seeds with plasma activated water to enhance germination, plant growth, and plant composition. Plasma Chem Plasma Process. :1–21
10. Rathore V, Nema SK (2023) Investigating the role of plasma-activated water on the growth of Freshwater Algae Chlorella Pyrenoidosa and Chlorella Sorokiniana. Plasma Chem Plasma Process. :1–25
11. Talviste R, Raud S, Jõgi I, Plank T, Raud J, Teesalu T (2019) Investigation of a he micro plasma-jet utilized for treatment of prostate cancer cells. Plasma Res Express 1(4):045002

12. Cheng J-H, He L, Sun D-W, Pan Y, Ma J (2023) Inhibition of cell wall pectin metabolism by plasma activated water (PAW) to maintain firmness and quality of postharvest blueberry. Plant Physiol Biochem. :107803
13. Flores-Silva PC, Ramírez-Vargas E, Palma-Rodriguez H, Neira-Velazquez G, Hernandez-Hernandez E, Mendez-Montealvo G et al (2023) Impact of plasma-activated water on the supramolecular structure and functionality of small and large starch granules. Int J Biol Macromol. :127083
14. Arda G, Hsu C-l (2023) Preservation of reactive species in frozen plasma-activated water and enhancement of its bactericidal activity through pH Adjustment. Plasma Chem Plasma Process. :1–20
15. Zhou Z, Li H, Qi Z, Liu D (2023) Biological and Chemical Reactivities of plasma-activated Water prepared at different temperatures. Plasma Chem Plasma Process. :1–18
16. Qiao D, Li Y, Pan J, Zhang J, Tian Y, Wang KJPC et al (2022) Effect of plasma activated Water in Caries Prevention: the Caries Related Biofilm Inhibition effects and mechanisms. Plasma Chem Plasma Process 42(4):801–814
17. Li Y, Pan J, Wu D, Tian Y, Zhang J, Fang J (2019) Regulation of Enterococcus faecalis biofilm formation and quorum sensing related virulence factors with ultra-low dose reactive species produced by plasma activated water. Plasma Chem Plasma Process 39:35–49
18. Pan J, Li Y, Liu C, Tian Y, Yu S, Wang K et al (2017) Investigation of cold atmospheric plasma-activated water for the dental unit waterline system contamination and safety evaluation in vitro. Plasma Chem Plasma Process 37:1091–1103
19. Qi Z, Tian E, Song Y, Sosnin EA, Skakun VS, Li T et al (2018) Inactivation of Shewanella putrefaciens by plasma activated water. Plasma Chem Plasma Process 38:1035–1050
20. Subramanian P, Rao H, Shivapuji AM, Girard-Lauriault P-L, Rao L (2021) Plasma-activated water from DBD as a source of nitrogen for agriculture: specific energy and stability studies. J Appl Phys. ;129(9)
21. Matějka F, Galář P, Khun J, Scholtz V, Kůsová K (2023) Mechanisms leading to plasma activated water high in nitrogen oxides. Phys Scr 98(4):045619
22. Corella Puertas E, Dzafic A, Coulombe S (2020) Investigation of the electrode erosion in pin-to-liquid discharges and its influence on reactive oxygen and nitrogen species in plasma-activated water. Plasma Chem Plasma Process 40:145–167
23. Sajib SA, Billah M, Mahmud S, Miah M, Hossain F, Omar FB et al (2020) Plasma activated water: the next generation eco-friendly stimulant for enhancing plant seed germination, vigor and increased enzyme activity, a study on black gram (Vigna mungo L). Plasma Chem Plasma Process 40:119–143
24. El Shaer M, Abdel-azim M, El-welily H, Hussein Y, Abdelghani A, Zaki A et al (2023) Effects of DBD Direct Air Plasma and gliding Arc Indirect plasma activated Mist on Germination, and physiological parameters of Rice seeds. Plasma Chemistry Plasma Processing
25. Wartel M, Faubert F, Dirlau I, Rudz S, Pellerin N, Astanei D et al (2021) Analysis of plasma activated water by gliding arc at atmospheric pressure: Effect of the chemical composition of water on the activation. J Appl Phys. ;129(23)
26. Rathore V, Desai V, Jamnapara NI, Nema SK (2022) Activation of water in the downstream of low-pressure ammonia plasma discharge. Plasma Res Express 4(2):025008
27. Xu H, Quan L, Liu Y, Zhang H, Shao M, Xie K (2022) Effect of external E× E and E× B configurations on an atmospheric-pressure plasma jet and plasma-activated water: experiments and simulations. Phys Plasmas. ;29(7)
28. Rathore V, Nema SK (2022) The role of different plasma forming gases on chemical species formed in plasma activated water (PAW) and their effect on its properties. Phys Scr 97(6):065003
29. Rathore V, Nema SK (2022) A comparative study of dielectric barrier discharge plasma device and plasma jet to generate plasma activated water and post-discharge trapping of reactive species. Phys Plasmas. ;29(3)
30. Xu H, Xu H, Huang Y, Wei Z, Zhang H, Shao M et al (2023) Enhanced water activation in gas–liquid two-phase flow using air plasma droplets. Phys Plasmas. ;30(5)
31. Pandey S, Jangra R, Ahlawat K, Mishra R, Mishra A, Jangra S et al (2023) Selective generation of nitrate and nitrite in plasma activated water and its physicochemical parameters analysis. Phys Lett A 474:128832
32. Rathore V, Jamnapara NI, Nema SK (2023) Enhancing the physicochemical properties and reactive species concentration of plasma activated water using an air bubble diffuser. Phys Lett A 482:129035
33. Chiu P-H, Cheng Y-C, Lua KB, Wu J-S (2023) DBD-Streamer Mode Transition of Atmospheric-pressure plasma Jet Applied on Water with varying Distance and AC Power. Phys Scr
34. Hoeben W, Van Ooij P, Schram D, Huiskamp T, Pemen A, Lukeš P (2019) On the possibilities of straightforward characterization of plasma activated water. Plasma Chem Plasma Process 39:597–626
35. Schmid-Wendtner M-H, Korting HC (2007) pH and skin care: Abw Wissenschafts
36. Korde Choudhari S, Chaudhary M, Bagde S, Gadbail AR, Joshi V (2013) Nitric oxide and cancer: a review. World J Surg Oncol 11:1–11

37. Falkenberg LJ, Bellerby RG, Connell SD, Fleming LE, Maycock B, Russell BD et al (2020) Ocean acidification and human health. Int J Environ Res 17(12):4563
38. Sumner M (1994) Measurement of soil pH: problems and solutions. Commun Soil Sci Plant Anal 25(7–8):859–879
39. Singh A, Agrawal M (2007) Acid rain and its ecological consequences. J Environ Biol 29(1):15
40. Guinotte JM, Fabry VJ (2008) Ocean acidification and its potential effects on marine ecosystems. Ann N Y Acad Sci 1134(1):320–342
41. Sivachandiran L, Khacef A (2017) Enhanced seed germination and plant growth by atmospheric pressure cold air plasma: combined effect of seed and water treatment. RSC Adv 7(4):1822–1832
42. Xu Y, Zhang Q, Chen H, Huang Y (2023) Understanding the interaction between erosion and corrosion of pipeline steel in acid solution of different pH. J Mater Res Technol 25:6550–6566
43. Ukpaka C, Wami E, Amadi S (2015) Effect of pollution on metal corrosion: a case study of carbon steel metal in acidic media. Curr Sci Perspect 1(4):107–111
44. Abdel-Gaber A, Abd-El Nabey B, Sidahmed I, El-Zayady A, Saadawy M (2006) Effect of temperature on inhibitive action of damsissa extract on the corrosion of steel in acidic media. Corrosion 62(4):293–299
45. Pang B, Liu Z, Wang S, Gao Y, Qi M, Xu D et al (2022) Alkaline plasma-activated water (PAW) as an innovative therapeutic avenue for cancer treatment. Appl Phys Lett. ;121(14)
46. Nisoa M, Sirisathitkul Y, Sirisathitkul C, DEVELOPMENT OF INDUSTRIAL PROTOTYPE FOR ACTIVATING WATER BY, PLASMA JET (2022). Proceedings of the Romanian Academy, Series A: Mathematics, Physics, Technical Sciences, Information Science. ;23(4)
47. Pekárek S (2017) Experimental study of nitrogen oxides and ozone generation by corona-like dielectric barrier discharge with airflow in a magnetic field. Plasma Chem Plasma Process 37(5):1313–1330
48. Rathore V, Patel S, Pandey A, Savjani J, Butani S, Dave H et al (2023) Methotrexate degradation in artificial wastewater using non-thermal pencil plasma jet. Environ Sci Pollution Res. :1–10
49. Rathore V, Nema SK (2021) Optimization of process parameters to generate plasma activated water and study of physicochemical properties of plasma activated solutions at optimum condition. J Appl Phys. ;129(8)
50. Rathore V, Patil C, Sanghariyat A, Nema SK (2022) Design and development of dielectric barrier discharge setup to form plasma-activated water and optimization of process parameters. Eur Phys J D 76(5):77
51. Qayyum A, Zeb S, Ali S, Waheed A, Zakaullah M (2005) Optical emission spectroscopy of abnormal glow region in nitrogen plasma. Plasma Chem Plasma Process 25:551–564
52. Shemansky D, Broadfoot A (1971) Excitation of N2 and N+2 systems by electrons—I. Absolute transition probabilities. J Quant Spectrosc Radiative Transf 11(10):1385–1400
53. Liu X, Chen F, Huang S, Yang X, Lu Y, Zhou W et al (2015) Characteristic and application study of cold atmospheric-pressure nitrogen plasma jet. IEEE Trans Plasma Sci 43(6):1959–1968
54. Liu F, Wang W, Wang S, Zheng W, Wang Y (2007) Diagnosis of OH radical by optical emission spectroscopy in a wire-plate bi-directional pulsed corona discharge. J Electrostat 65(7):445–451
55. Baker J (2008) Transition probabilities for one electron atoms, technical note. Natl Inst Stand Technol, Washington, DC
56. Rathore V, Nema SK (2023) Selective generation of reactive oxygen species in plasma-activated water using CO2 plasma. J Vacuum Sci Technol A. ;41(4)
57. Thirumdas R, Kothakota A, Annapure U, Siliveru K, Blundell R, Gatt R et al (2018) Plasma activated water (PAW): Chemistry, physico-chemical properties, applications in food and agriculture. Trends food Sci Technol 77:21–31
58. Tschang C-YT, Thoma M (2019) In vitro comparison of direct plasma treatment and plasma activated water on Escherichia coli using a surface micro-discharge. J Phys D 53(5):055201
59. Shen J, Tian Y, Li Y, Ma R, Zhang Q, Zhang J et al (2016) Bactericidal effects against S. Aureus and physicochemical properties of plasma activated water stored at different temperatures. Sci Rep 6(1):28505
60. Kaushik NK, Ghimire B, Li Y, Adhikari M, Veerana M, Kaushik N et al (2019) Biological and medical applications of plasma-activated media, water and solutions. Biol Chem 400(1):39–62
61. Tian Y, Ma R, Zhang Q, Feng H, Liang Y, Zhang J et al (2015) Assessment of the physicochemical properties and biological effects of water activated by non-thermal plasma above and beneath the water surface. Plasma Processes Polym 12(5):439–449
62. Zhang Q, Ma R, Tian Y, Su B, Wang K, Yu S et al (2016) Sterilization efficiency of a novel electrochemical disinfectant against Staphylococcus aureus. Environ Sci Technol 50(6):3184–3192
63. Xiang Q, Kang C, Niu L, Zhao D, Li K, Bai Y (2018) Antibacterial activity and a membrane damage mechanism of plasma-activated water against Pseudomonas deceptionensis CM2. Lwt 96:395–401

64. Lu P, Boehm D, Bourke P, Cullen PJ (2017) Achieving reactive species specificity within plasma-activated water through selective generation using air spark and glow discharges. Plasma Processes Polym 14(8):1600207
65. Ma R, Wang G, Tian Y, Wang K, Zhang J, Fang J (2015) Non-thermal plasma-activated water inactivation of food-borne pathogen on fresh produce. J Hazard Mater 300:643–651
66. Vlad I-E, Anghel SD (2017) Time stability of water activated by different on-liquid atmospheric pressure plasmas. J Electrostat 87:284–292
67. Machala Z, Tarabova B, Hensel K, Spetlikova E, Sikurova L, Lukes P (2013) Formation of ROS and RNS in Water Electro-S prayed through transient spark discharge in Air and their Bactericidal effects. Plasma Processes Polym 10(7):649–659
68. Jablonowski H, von Woedtke T (2015) Research on plasma medicine-relevant plasma–liquid interaction: what happened in the past five years? Clin Plasma Med 3(2):42–52
69. Oehmigen K, Winter J, Hähnel M, Wilke C, Brandenburg R, Weltmann KD et al (2011) Estimation of possible mechanisms of Escherichia coli inactivation by plasma treated sodium chloride solution. Plasma Processes Polym 8(10):904–913
70. Cao X, Novitski D, Holdcroft S (2019) Visualization of hydroxide ion formation upon electrolytic water splitting in an anion exchange membrane. ACS Mater Lett 1(3):362–366
71. Sakai H, Fujiwara T, Kumamaru T (1996) Determination of inorganic anions in water samples by ion-exchange chromatography with chemiluminescence detection based on the neutralization reaction of nitric acid and potassium hydroxide. Anal Chim Acta 331(3):239–244
72. Steehler J, Chemistry L, Brown H, Eugene LeMay Jr., and Bruce E. Bursten ChemistryChemical Reactivity, by, Kotz JC, Treichel P (1997) Jr. Journal of Chemical Education. ;74(4):378
73. Suchak NJ, Jethani K, Joshi JB (1990) Absorption of nitrogen oxides in alkaline solutions: selective manufacture of sodium nitrite. Industrial Eng Chem Res 29(7):1492–1502
74. Rezaei F, Gorbanev Y, Chys M, Nikiforov A, Van Hulle SW, Cos P et al (2018) Investigation of plasma-induced chemistry in organic solutions for enhanced electrospun PLA nanofibers. Plasma Processes Polym 15(6):1700226
75. Hibbert A, Biémont E, Godefroid M, Vaeck N (1991) E1 transitions of astrophysical interest in neutral oxygen. J Phys B: at Mol Opt Phys 24(18):3943
76. Hiroyuki N (1968) Excitation of N2+, O2+and CO2+band by electron impact. J Phys Soc Jpn 24(1):130–143

Authors and Affiliations

Vikas Rathore[1] · Karaket Watanasit[2] · Suttirak Kaewpawong[2] · Dhammanoon Srinoumm[2] · Arlee Tamman[3] · Dheerawan Boonyawan[4] · Mudtorlep Nisoa[2,5]

✉ Mudtorlep Nisoa
nmudtorl@wu.ac.th

[1] Atmospheric Plasma Division, Institute for Plasma Research (IPR), Gandhinagar 382428, Gujarat, India

[2] Functional Materials and Nanotechnology Center of Excellence, Walailak University Nakhon, Si Thammarat 80160, Thailand

[3] Center of Excellence in Engineering and Nuclear Technology, Institute of Nuclear Technology, Nakhon Nayok 26120, Thailand

[4] Department of Physics and Materials Science, Faculty of Science, Chiang Mai University, Chiang Mai 50200, Thailand

[5] Division of Physics, School of Science, Walailak University, Nakhon Si Thammarat 80160, Thailand